EXCITATION TESTS OF SEMI-ACTIVE SEISMIC ISOLATION SYSTEM USING MR DAMPERS

Eiji SATO[1] and Takafumi FUJITA[2]

ABSTRACT: A semi-active seismic isolation system using a controllable damper was developed to decrease the relative displacement between the ground and a superstructure during an earthquake. This study examines a semi-active seismic isolation system that uses a magneto-rheological (MR) damper. Despite its benefits, the MR damper's response to the mechanism is delayed, which negatively impacts control performance. To solve this problem, semi-active seismic isolation control methods that take the MR damper delay into consideration were examined. This paper outlines the results of excitation tests on the semi-active seismic isolation system with the MR damper using these control methods.

Keywords: *semi-active seismic isolation system, MR damper, excitation test*

INTRODUCTION

Several base-isolated buildings have been constructed using passive isolation systems to decrease response acceleration of superstructures during an earthquake (Fujita 1991a). The trade-off is that large relative displacement is inevitable in a passive seismic isolation system in order to decrease the response acceleration of the superstructures.

To solve this trade-off problem, a semi-active seismic isolation system using a controllable friction damper was developed (Fujita 1991b, Fujita 1992). This study examines a semi-active seismic isolation system with an MR damper that uses magneto-rheological (MR) fluid as the hydrualic fluid. The flow resistance of the MR fluid is easily changed by altering the magnetic field; however, an MR damper has a delayed response to the mechanism, and this delay negatively influences the semi-active seismic isolation performance.

To solve this delay problem, semi-active seismic isolation control methods were examined. These were based on the Linear Quadratic (LQ) optimum regulator theory and the Instantaneous Optimal Control (IOC) algorithm and designed to take the delay of the MR damper into consideration. Several experiments were conducted to determine the characteristics of the MR damper, and a numerical model was developed using the results of these experiments. Excitation tests were conducted on the semi-active seismic isolation system with the MR damper, and the LQ and the IOC algorithms were used to establish the seismic isolation and the relative displacement reduction based on the delay of the MR damper.

This paper reports the results of the characterization experiments and the excitation tes ts.

MR DAMPER

The MR damper is shown in Figure 1 and its configuration is presented in Figure 2. Table 1 lists the specifications of the MR damper used in the experiments. The MR damper is an energy-absorbing device that uses the flow resistance of the fluid enclosed in the cylinder as in an oil damper. The MR fluid, enclosed in a right and left cylinder, passes through an orifice in the bypass flow under the

[1] Cooperative Research Fellow
[2] Professor

damper. The magnetic field is changed by a coil installed in the bypass flow. This changes the flow resistance of the MR fluid, and the energy absorption characteristics (damping force) of the MR damper changes. Therefore, the damping force of the MR damper (generation force) can be changed by controlling the current applied to the coil, but this response is not immediate due to the amount of time it takes for the input current to effect a change in the magnetic field and a subsequent change in the MR fluid flow resistance. This delay negatively affects the performance of the semi-active seismic isolation controls in no small way.

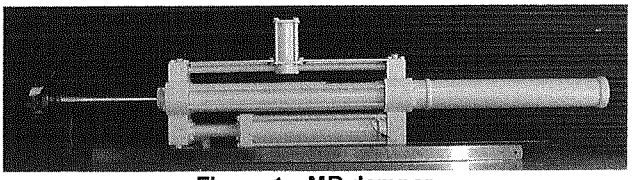

Figure 1 MR damper

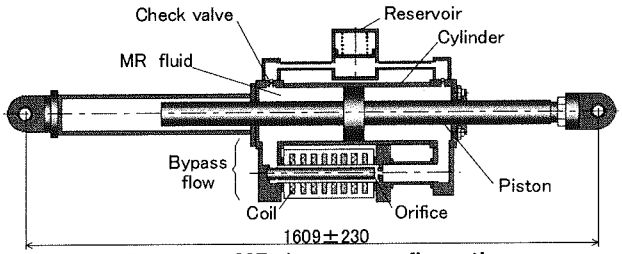

Figure 2 MR damper configuration

Table 1 MR damper Specifications

Item	Specification
MR fluid	LORD MRF-132AD (1 ℓ)
Rated force	10kN
Rated displacement	±230mm
Rated input current	4A
Coil resistance	31.5 Ω
Inductance	70.2 mH
Number of turns	280

MR DAMPER CHARACTERIZATION EXPERIMENT

Experimental apparatus and instrumentation

The excitation wave, excitation velocity, and input current to the coil were changed, and various data about the MR damper were collected. This resulted in a better understanding of the MR damper. The MR damper was excited with the hydraulic actuator. The experiment layout is shown in Figure 3, while the experimental apparatus and instrumentation system are shown in Figure 4. The damping force was measured with the load cell set between the rod and the hydraulic actuator. Displacement was measured with the displacement transducer. Input current to the coil was calculated from the amount of voltage applied to the amplifier.

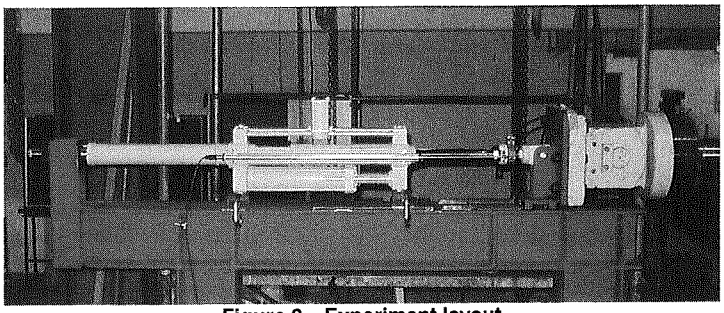

Figure 3 Experiment layout

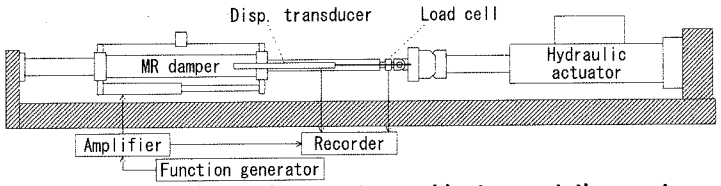

Figure 4 Experimental apparatus and instrumentation system

Velocity- dependence test

The damper was constantly excited by a sine wave input current applied to the coil to confirm the hysteretic behavior and the effect of the MR damper piston velocity on the generation force. Figure 5 depicts the results when 0A, 0.5A, 1.0A, 1.5A, 2.0A, or 2.5A of current was input, and the MR damper was excited by a sine wave of 20cm/s.

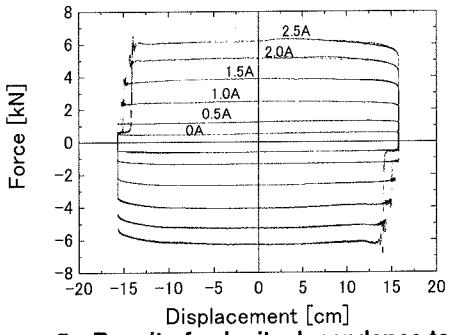

Figure 5 Result of velocity dependence test

The test confirmed that the MR damper is a Bingham model that operates not by velocity-proportional damping alone, but in parallel with the coulomb friction element. Moreover, it was confirmed that a dead zone is created when the MR damper's piston changes direction. This dead zone results from the delayed reaction of check valves installed in the MR damper.

Response tests

Step-response and frequency-response experiments were conducted to confirm the response characteristics of the MR damper between application of the input current and change in the generation force.

In the step-response experiment, the input current was applied from 0A to 3A, as in the step wave, and the generation force at that time was measured. Figure 6 shows the result of the step-response experiment.

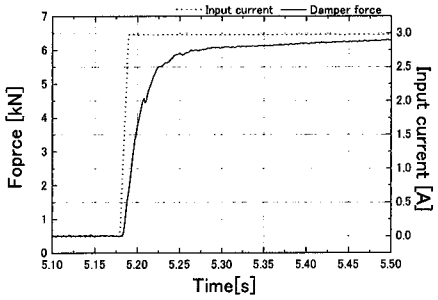

Figure 6 Result of step-response experiment

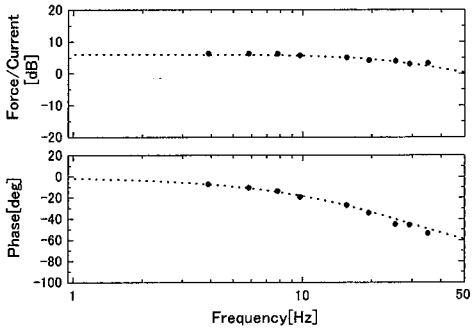

Figure 7 Result of frequency-response experiment

The generation force intensified about 0.01s after the input current was increased, and converged about 0.1s after becoming the input current stationary state.

Figure 7 illustrates the results of the frequency-response experiment. Here, the gain was calculated from the input as the current to the MR damper and the output as the generation force. The dotted line in these figures shows the identification result in the first-order leg. The gain is almost flat up to 35Hz, and the phase has a delay of about 20° at 10Hz. Moreover, it was confirmed that the identification result by the first-order leg agreed well with the experimental results.

Generation force fluctuation test

In order to confirm the relationship between the MR damper's generation force and the input current, experiments in which the input current was changed from 0 to 2.5A, as the sine wave, were conducted. Figure 8 shows this test result.

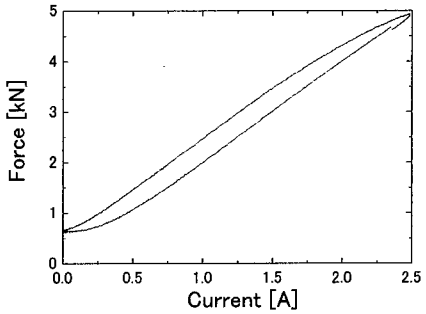

Figure 8 Input current and generation force relationship

There is hysteresis between the input current and the generation force due to the delay between changes to the input current and the resulting generation force. The tests also confirmed that the MR damper is versatile enough to produce a force change band from about 0.7kN to 5kN.

MR DAMPER ANALSYS MODELE

The results of the characteristic experiments show that the MR damper model combines the Bingham model and the dead zone, as shown in Figure 9.

The delay of the MR damper was modeled in the following first-order leg.

$$T_L \dot{f}(t) + f(t) = f'(t) \qquad (1)$$

where T_L is a time constant and f is the generation force by the MR damper. The Linear Quadratic (LQ) optimum regulator theory and the Instantaneous Optimal Control (IOC) algorithm were used as the semi-active control theories.

The semi-active seismic isolation system using the MR damper is modeled as a single degree of freedom system, as depicted in Figure 10. The equation of motion of the model is shown below.

$$m\ddot{x} + c\dot{x} + kx + \mathrm{sgn}(\dot{x})f = -m\ddot{z} \qquad (2)$$

where m is the mass of the building, c is the damping coefficient, k is the spring constant, x is the relative displacement, and f is the generation force by the MR damper.

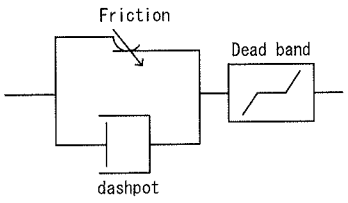

Figure 9 MR damper model

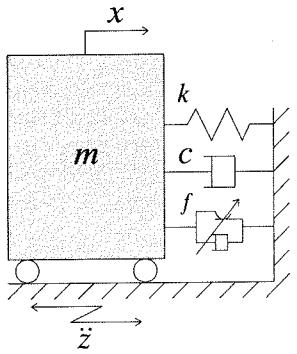

Figure 10 Seismic isolation building model

Linear Quadratic optimum regulator theory

The optimal generated force is obtained using the LQ. A performance index J is defined as follows (assuming that $u = f$):

$$J = \int_0^\infty \left\{\alpha(\ddot{x} + \ddot{z})^2 + \beta x^2 + \gamma u^2\right\} dt \qquad (3)$$

where α, β, and γ are weighting coefficients.

The expansion state equation is derived using expression (1) and the equation that linearizes expression (2). The LQ problem is therefore solved, and the following optimal control force u^* is obtained:

$$u^*(t) = -\mathbf{F}_b\mathbf{X}(t)\ , \quad \mathbf{F}_b = \mathbf{R}^{-1}\mathbf{B}^T\mathbf{P} \qquad (4)$$

where $\mathbf{X}(t)$ and $\mathbf{B}$ are the state variable vector and the control matrix of the expansion state equation, $\mathbf{R}$ is the weighting matrix of the quadratic form performance function, and $\mathbf{P}$ is the root of the Riccati algebraic equation. When the semi-active control using the damping force of the MR damper is considered, the direction of the force generated by the damper depends on the conditions below.

$$u = \begin{cases} u^* & (u^* \cdot \dot{x} > 0) \\ 0 & (u^* \cdot \dot{x} < 0) \end{cases} \qquad (5)$$

Instantaneous Optimal Control

When the MR damper is used, the equation of motion of the seismic isolation system is nonlinear. The IOC, which is effective on a nonlinear system, is used to obtain the optimal input. The performance index $J(t)$ of the IOC is defined as follows:

$$J(t) = q_v \dot{x}^2(t) + q_d x^2(t) + q_f f^2(t) + I^2(t) \tag{6}$$

where $q_v \geq 0$, $q_d \geq 0$, and $q_f \geq 0$ are weighting coefficients. $I(t)$ is the input current of the MR damper and is shown below.

$$u(t) = \alpha_0 + \alpha_1 I(t) \tag{7}$$

where α_0 and α_1 are coefficients obtained from the experiments.

The optimal input current $I^*(t)$ to minimize the performance function $J(t)$ is given as follows:

$$I^*(t) = -\frac{\Delta t \alpha_1 q_f}{2T_L + \Delta t} f(t) + \frac{\alpha_1 q_v \Delta t^2 \operatorname{sgn}(\dot{x}(t))}{2m(2T_L + \Delta t)\left(1 + \frac{\Delta t^2}{6}\omega^2 + \Delta t \zeta \omega\right)} \dot{x}(t)$$
$$+ \frac{\alpha_1 q_d \Delta t^3 \operatorname{sgn}(\dot{x}(t))}{6m(2T_L + \Delta t)\left(1 + \frac{\Delta t^2}{6}\omega^2 + \Delta t \zeta \omega\right)} x(t) \tag{8}$$

SHAKE-TABLE TESTS OF SEMI-ACTIVE SEISMIC ISOLATION SYSTEM

Test building model and control system

The building model used for the tests consists of a steel skeleton frame and steel plate weights and is supported by four linear bearings. Figure 11 depicts the test building model. The superstructure and base frame are connected with coil springs and the MR damper. The total mass of the superstructure is 6350 kg. The first mode natural frequency of the isolation system is 0.33 Hz.

The control system consists of sensors, DSP, A/D-D/A converters, and amplifier. The input voltage calculated by DSP is applied to the amplifier. Figure 12 illustrates the control system.

Test result

In the shake-table tests, inputs of 100cm/s^2, 200cm/s^2 and 300cm/s^2 were used to generate the maximum acceleration of El Centro NS (1940, Imperial Valley Earthquake).

Figure 13 illustrates the test results when the semi-active isolation controller is designed using the LQ, and Figure 14 illustrates the test results based on the IOC design. The weighting coefficients of the performance index are selected so that the response acceleration can be smaller in LQ reduce acc. and IOC reduce acc., and the relative displacement can be smaller in LQ reduce dis. and IOC reduce dis. of these figures. Passive 1 and Passive 2 in the figures indicate the passive seismic isolation using the MR damper with a constant input current. In the Passive 1 (Passive 2) case, the input current is set to begin to move the MR damper if the input acceleration of the shake table exceeds 10cm/s^2 (25cm/s^2). The results of the LQ and the IOC controller designs that did not take the MR damper delay into consideration are also shown in these figures for comparison.

Almost the same performance, in which response acceleration is decreased, is demonstrated with each semi-active control theory and the passive seismic isolation. However, all semi-active control theories decrease the relative displacement by about 60% more than the passive seismic isolation.

Relative displacement performance was significantly better when the semi-active control theory considered the MR damper delay compared to the one that did not, especially in the IOC design.

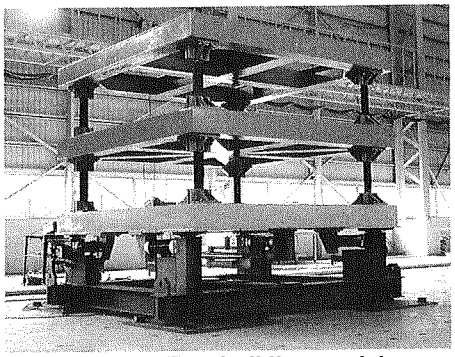

Figure 11 Test building model

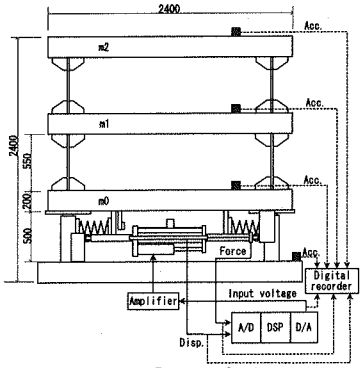

Figure 12 Control system

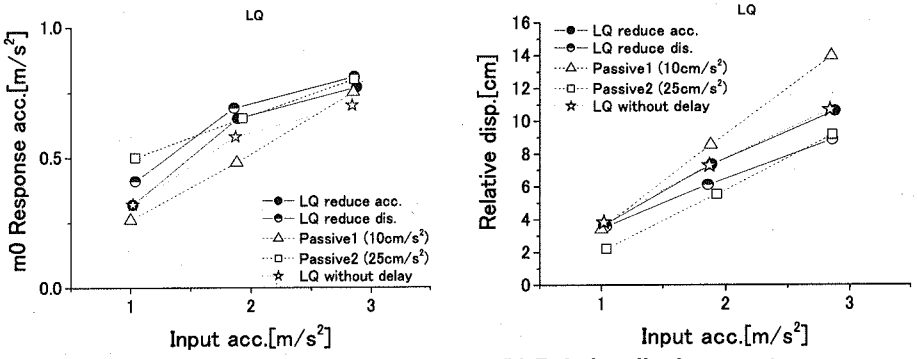

(a) Response acceleration **(b) Relative displacement**

Figure 13 Results with LQ

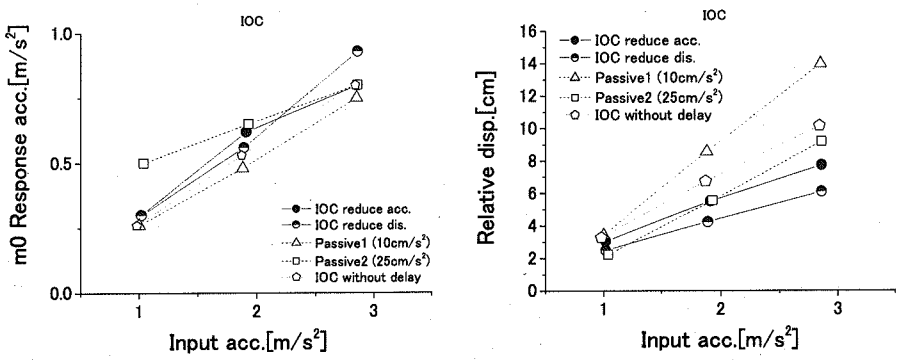

(a) Response acceleration **(b) Relative displacement**

Figure 14 Results with IOC

Figure 15 illustrates the time histories in LQ reduce acc., IOC reduce acc. and Passive 1. The input is EL Centro NS of 300cm/s^2. These figures also show the simulation results. The simulation results agree with the experimental results, confirming that the analysis model is valid.

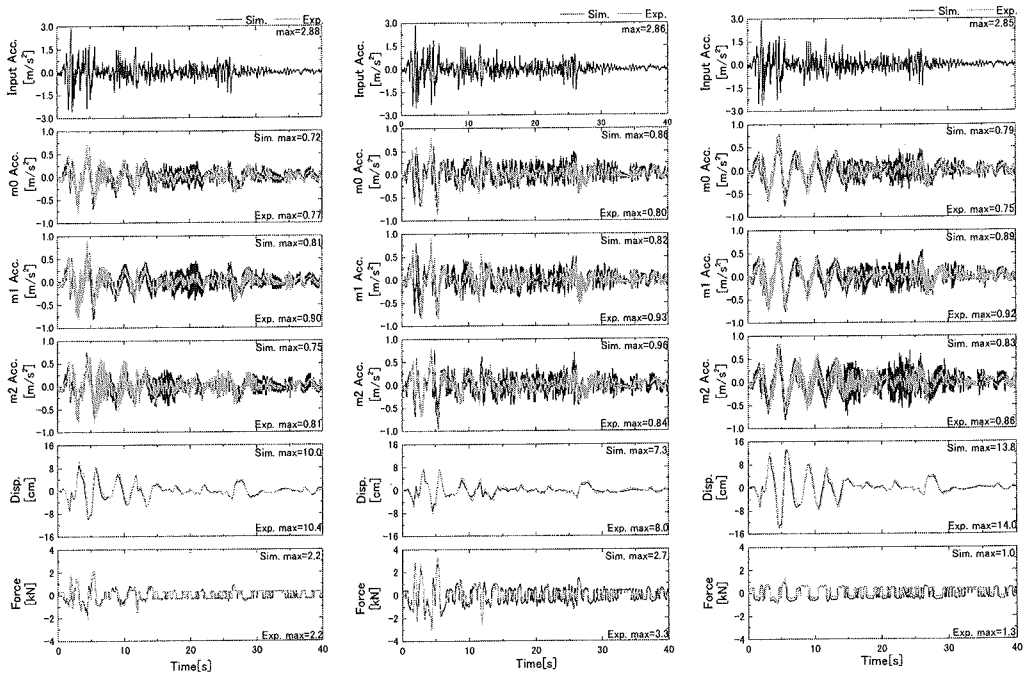

Figure 15 Time histories of responses of semi-active and passive systems (Experimental and simulation results)

CONCLUSIONS

An actual MR damper was manufactured for a semi-active seismic isolation system, and experiments were conducted to determine its characteristic traits. The results confirmed that the MR damper combines the Bingham model and the dead zone created when the MR damper's piston changes direction, and that the MR damper is versatile enough to produce a force change band from about 0.7kN to 5kN. In addition, the MR damper was modeled.

Shake-table tests were conducted on the semi-active isolation system that uses the MR damper. The tests confirmed that the semi-active seismic isolation system using the MR damper with the LQ or IOC controller design that takes the MR damper delay into consideration performs better than both the passive seismic isolation system and controller designs that do not consider the MR damper delay. The simulation results of the semi-active seismic isolation system using the MR damper agreed with the shake table test results as well, which confirmed the validity of the MR damper analysis model and the seismic isolation building.

References

1) Fujita, T. (1991a) "Research, development and application of seismic isolation systems in Japan, Proceeding of the International Meeting on Earthquake Protection of Builgings" Ancona, Italy,6-8, June, 77/C-90/C.

2) Fujita, T., Kabeya, K., Hayamizu, Y., Aizawa, S., Higashino, M., Kubo, T., Haniuda, N., and Mori, T., (1991b). "Semi-active seismic isolation system using controllable friction damper (1st report, Development of controllable friction damper and fundamental study of semi-active control system)" Trans. of Japan Soc. Mech. Eng. , 57, 536 Ser.C, 1122-1128 (in Japanese).

3) Fujita, T., Shimazaki, M., Hayamizu, Y., Aizawa, S., Higashino, M., Kubo, T., and Haniuda, N. (1992) "Semi-active seismic isolation system using controllable friction damper (2nd report, Study

of the system with distributed controllable friction dampers)" Trans. of Japan Soc. Mech. Eng. , 58, 551 Ser.C, 2012-2016 (in Japanese).
4) Sato, E., Fujita, T., (2002) "Fundamental Analysis for Semi-active Seismic Isolation System with Controllable Friction Damper Using Piezoelectric Actuators" Bull. ERS, No. 35, 21-30.
5) Sato, E., Fujita, T., (2003) "Experiments of Controllable Friction damper Using Piezoelectric Actuators for Semi-Active Seismic Isolation System" Bull. ERS, No. 36, 57-70.
6) Sato, E., Fujita, T., (2004) "Excitation Test for Experimental Model Semi-Active Seismic Isolation System with Controllable Friction Damper Using Piezoelectric Actuators" Bull. ERS, No. 37, 3-10.